THE JOURNAL OF PHYSICAL CHEMISTRY A
A JOURNAL OF THE AMERICAN CHEMICAL SOCIETY

pubs.acs.org/JPCA
Article

Aqueous Radical Initiated Oxidation of an Organic Monolayer at the Air−Water Interface as a Proxy for Thin Films on Atmospheric Aerosol Studied with Neutron Reflectometry

Stephanie H. Jones,* Martin D. King,* Adrian R. Rennie, Andrew D. Ward, Richard A. Campbell, and Arwel V. Hughes

Cite This: J. Phys. Chem. A 2023, 127, 8922−8934
Read Online

ABSTRACT: Neutron reflectometry has been used to study the radical initiated oxidation of a monolayer of the lipid 1,2-distearoyl-*sn*-glycero-3-phosphocholine (DSPC) at the air−solution interface by aqueous-phase hydroxyl, sulfate, and nitrate radicals. The oxidation of organic films at the surface of atmospheric aqueous aerosols can influence the optical properties of the aerosol and consequently can impact Earth's radiative balance and contribute to modern climate change. The amount of material at the air−solution interface was found to decrease on exposure to aqueous-phase radicals which was consistent with a multistep degradation mechanism, i.e., the products of reaction of the DSPC film with aqueous radicals were also surface active. The multistep degradation mechanism suggests that lipid molecules in the thin film degrade to form progressively shorter chain surface active products and several reactive steps are required to remove the film from the air−solution interface. Bimolecular rate constants for oxidation via the aqueous phase OH radical cluster around 10^{10} dm^3 mol^{-1} s^{-1}. Calculations to determine the film lifetime indicate that it will take ∼4−5 days for the film to degrade to 50% of its initial amount in the atmosphere, and therefore attack by aqueous radicals on organic films could be atmospherically important relative to typical atmospheric aerosol lifetimes.

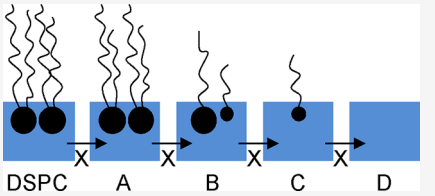

INTRODUCTION

Atmospheric aerosols exist as complex chemical mixtures in the troposphere[1−6] and are known to influence the Earth's climate, directly by scattering and absorbing radiation and indirectly through formation of cloud condensation nuclei (CCN) and ice nuclei (IN) and their resultant impact on cloud properties.[7,8] The aerosol contribution to radiative forcing of the climate remains a major source of uncertainty, and it is therefore necessary to study how aerosol and cloud droplet properties change as a result of common tropospheric reactions such as oxidation.

Thin organic films exist on the surface of aerosols at the air−water interface and the air−solid interface.[9−18] Marine aerosol, formed via bubble bursting action over the ocean, is a well-known abundant tropospheric aerosol coated with an organic surface active film.[9,10,14] The coating originates from organic material, including lipids, present in the sea surface microlayer (tens to hundreds of micrometers of the uppermost ocean).[10,19,20] Lipids that are present in plant waxes and become airborne by wind action are also a terrestrial source of thin organic films on aerosols.[21] Such organic coatings are believed to form an encapsulating film on the aerosol surface and thus play a central role in aerosol chemistry affecting surface tension and hygroscopic (ability to uptake water) properties.[9−12,22,23] Films on atmospheric aerosols change their light scattering properties which may change their ability to change the Earth's albedo as demonstrated by simple 1D radiative-transfer models.[24] The presence of the film at the aerosol's interface and its thickness may be more important than the film's molecular identity.[25] Atmospheric aerosol is readily oxidized in the atmosphere via a number of gaseous and liquid-phase oxidants,[26,27] resulting in changes in aerosol chemical, physical, and optical properties.[28] Thin organic films present on the surface of aerosol may also be readily oxidized, causing changes in coated aerosol properties, such as hygroscopicity, optical properties, and aerosol atmospheric lifetime.[7,29−33] Several studies have suggested that the oxidation of an organic film at the air−water interface may influence the formation and activation of cloud droplets.[22,30,31,33−36] As an example, King et al.[33,35] demonstrated the oxidation of an oleic acid film at the air−water interface as a proxy for an organic coating on aerosol and found that the critical supersaturation required for droplet formation will be lowered as a result.

Atmospheric oxidants exist in both the gaseous and aqueous phase; common gas phase oxidants include ozone,[37,38]

Received: June 7, 2023
Revised: September 12, 2023
Published: October 13, 2023

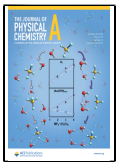

https://doi.org/10.1021/acs.jpca.3c03846
J. Phys. Chem. A 2023, 127, 8922−8934

hydroxyl,[39] and nitrate radicals[40] and common aqueous phase cloudwater oxidants include hydroxyl, sulfate, and nitrate radicals.[41] The authors acknowledge the presence of other oxidants such as aqueous ozone and carbonate ($CO_3^{\bullet-}$) present in terrestrial waters[42] and emphasize that the current study focuses on processes occurring in cloudwater. A coated aerosol could be oxidized from the gaseous phase above the film, i.e., from the "top-down",[25,35] or from the aqueous phase below the film, i.e., from the "bottom-up". Oxidation from the "bottom-up" has been shown for solid films and radicals generated from the solid phase.[43] Karagulian et al.[43] studied the oxidation of a solid monolayer of the lipid 1-oleoyl-2-palmitoyl-*sn*-glycero-3-phosphocholine (OPPC) coated on a mixture of $NaNO_2$ and NaCl. OH radicals were formed on illumination of the system, and oxidation of the OPPC film was observed using diffuse reflection infrared Fourier transform spectrometry (DRIFTS) and matrix assisted ionization mass spectrometry (MALDI). The study suggested that similar reactions could also occur for aqueous aerosols coated with an organic film. Jones et al.[44] used X-ray reflectivity to study the oxidation of atmospheric films using material extracted from atmospheric filter samples at the air−solution interface and conducted experiments from the "bottom-up" using the aqueous phase radicals OH and nitrate radical to demonstrate that the atmospheric film was susceptible to aqueous reaction.

It is known that aqueous cloud processes oxidize thin films, but little is known about the kinetics. Therefore, in order to assess the importance of aqueous-phase oxidation of thin films and to determine the film lifetime with respect to oxidation, the investigation of the aqueous phase oxidation of a well-defined organic film of the lipid 1,2-distearoyl-*sn*-glycero-3-phosphocholine (DSPC) by the common cloudwater aqueous phase radicals, hydroxyl ($^{\bullet}OH$),[45−48] sulfate ($SO_4^{\bullet-}$)[27,41] and nitrate ($NO_3^{\bullet}$),[27,41,49] was performed. The reactions were probed by a series of neutron reflectometry experiments using films spread on the surface of solutions in a Teflon trough.

Neutron reflectometry is a surface reflection technique that can provide information about the physical properties of molecular monolayers and reaction kinetics at the air−solution interface.[50−52] In the present work, neutron reflectometry was used to follow the surface coverage and estimate the thickness of the films at the air−solution interface as they react. Previous neutron reflectometry studies have been successfully conducted on the gas-phase oxidation of atmospherically relevant monolayers at the air−water interface.[25,35,44,53−55] X-ray reflectivity has also been used to study the susceptibility of real atmospheric films[44] to oxidation from the gaseous and aqueous phase. The lipid DSPC was chosen for the current study as it is a naturally occurring phosphocholine lipid that forms organic films[56,57] with a well-known chemical structure and is therefore well suited to kinetic studies.

The following aqueous phase reactions were studied using neutron reflectometry to follow the decay of material (DSPC film and resultant products) at the air−solution interface:

$$^{\bullet}OH_{(aq)} + DSPC_{(surf)} \rightarrow \text{products} \quad \text{(R1)}$$

$$SO_4^{\bullet-}{}_{(aq)} + DSPC_{(surf)} \rightarrow \text{products} \quad \text{(R2)}$$

$$NO_3^{\bullet}{}_{(aq)} + DSPC_{(surf)} \rightarrow \text{products} \quad \text{(R3)}$$

where "surf" is used to indicate the air−solution interface.

The oxidative loss of DSPC from the air−solution interface was subsequently kinetically modeled to reproduce the surface coverage as a function of reaction time. A bimolecular rate constant was determined for the loss of surface-active material at the air−solution interface, thus allowing the calculation of a film lifetime with respect to radical oxidation in the atmosphere. Comparison of the film lifetime with typical atmospheric aerosol residence times allows the importance of such aqueous phase radical reactions to be assessed and informs on whether such reactions should be included in atmospheric and aerosol/cloud models.

EXPERIMENTAL METHODS

The section described here includes an introduction to neutron reflectometry and the associated experimental setup used in the neutron reflection experiments. An explanation of aqueous radical generation is provided as well as a description of the calculation of the radical steady-state concentration.

Neutron Reflectometry. Neutron reflectometry was used to study a monolayer film at the air−solution interface.[50] Specular neutron reflection allows the determination of the neutron refractive index profile normal to the air−solution interface.[51] The reflectivity of the film can be modeled and compared to experimental data to obtain information on the amount and thickness of material at the air−solution interface.

Measurements were made at the ISIS neutron source at the Rutherford Appleton Laboratory, Oxfordshire, UK, using the SURF reflectometer[58] and at the Institut Laue-Langevin (ILL), Grenoble, France, using the FIGARO reflectometer.[59] At ISIS, neutron reflection was recorded at an angle of 1.5° to the horizontal using a wavelength range of 0.5−6 Å. At the ILL, neutron reflection was recorded at an incident angle of 0.62° to the horizontal with a wavelength range of 2−20 Å and at an incident angle of 3.8° to the horizontal with a wavelength range of 2−30 Å.

The application of the neutron reflection technique to species at the air−water interface has been described by Lu et al.[50] and therefore will only be described briefly here. Neutron reflectivity, R, is measured as a function of the momentum transfer, Q, of the neutron[58] where Q is defined as

$$Q = \frac{4\pi \sin\theta}{\lambda} \quad \text{(A)}$$

where λ is the neutron wavelength and θ is the incident angle of the neutron beam.

Neutron reflectivity[50] for a monolayer of deuterated material at the air−water interface is approximately given by

$$R = \frac{16\pi^2}{Q^4}(2\rho)^2 \sin\left(\frac{Q\delta}{2}\right)^2 \quad \text{(B)}$$

where δ is the film thickness and ρ is the scattering length density[51] defined as

$$\rho = \sum_i nb_i \quad \text{(C)}$$

where b is the neutron scattering length of a nucleus and n is the number density of that element.[48] The value of b for fully deuterated DSPC ($C_{44}H_5NO_8PD_{83}$) used in this study is 888.34 fm based on values of b for individual elements.[60] The reflectivity data were normalized using the intensity spectrum of the direct beam of neutrons, and the absolute reflectivity was

https://doi.org/10.1021/acs.jpca.3c03846
J. Phys. Chem. A 2023, 127, 8922−8934

determined using a scale factor obtained from measuring the reflectivity of pure D_2O in the trough.

Isotopes of the same element typically have different neutron scattering lengths[60] where b depends on the interaction between the nucleus of an atom and a neutron.[61] The difference in bound coherent scattering length between hydrogen and deuterium is distinct, $b = -3.74$ fm for hydrogen and $b = 6.67$ fm for deuterium, whereas the chemical properties are the same. Specific chemical moieties of a molecule can be selectively deuterated in order to highlight the deuterated parts by producing a strong contrast between the film, subphase and air.[50] The subphase is the medium below the film, i.e., the monolayer film to be studied is spread on top of the subphase, a radical precursor solution in the experiments described here. In our study, the reflectivity of the film was increased relative to the air and subphase by using fully deuterated DSPC ($C_{44}H_5NO_8PD_{83}$) in order to achieve a large scattering length density ($\rho = 7.17 \times 10^{-6}$ Å^{-2}, calculated from values given by Hollinshead et al.[62]) in comparison to that of the subphase. The subphase had a scattering length density of zero (effectively the same as the air above the film) and was therefore null reflecting. A solution of so-called null reflecting water (NRW) consists of D_2O and H_2O in the volume proportion 8.1% and 91.9%, respectively. In the current experiment, aqueous radicals were generated photolytically from the subphase, and consequently, the volume ratio of D_2O and H_2O in the subphase was slightly adjusted to account for the scattering length density of the radical precursor chemicals to achieve an overall value of zero scattering length density. A monolayer of fully deuterated DSPC was spread on top of the null reflecting radical precursor subphase contained in the trough, and the specular neutron reflection signal was dominated by reflection from the monolayer film. Neutron reflectometry measures the combined amount of reactant and any insoluble, involatile, surface-active reaction product that remains at the air−solution interface, meaning it is a convolution of the remaining reactants and any products that have not yet dissolved or evaporated.

In the current study, neutron reflectivity as a function of Q was typically recorded continuously in intervals of 300 or 900 s (i.e., time to record one reflectivity profile R vs Q). Each kinetic run monitoring reactions R1−R3 was ∼50 000 s in duration. The experimental reflectivity versus the momentum transfer was modeled with a single uniform layer using the Abelès formalism,[63] which allows determination of the scattering length density and thickness of the deuterated material at the air−solution interface.

Scattering length density ρ, and film thickness δ, can be related to the scattering length b, of a molecule of a film composed entirely of the same molecule, and its surface coverage, Γ, by[35]

$$\Gamma b = \rho\delta \tag{D}$$

However, the scattering length, b, is not constant in a reacting system where the molecule does not leave the air−solution interface, and a mixture of different product molecules may also be present at the air−solution interface with different neutron scattering lengths, contributing to the overall neutron reflectivity. Therefore, the scattering length per unit area, $\rho\delta$, of all of the material at the air−solution interface is kinetically followed as a function of time, $\rho_t\delta_t$. As kinetics is the focus of the present study, the quantity

$$\frac{\rho_t\delta_t}{\rho_{t=0}\delta_{t=0}} \tag{E}$$

was followed as a function of time, where $\rho_{t=0}\delta_{t=0}$ is the product of the scattering length density and film thickness at time zero.

As will be detailed in the Multistep Degradation Kinetics section, to fit the variation of *equation E* to individual molecular components making up the film with time, the weighted sum of the individual products of scattering length, b, and surface coverage, Γ, for each component need to be considered.

MOTOFIT[64] was used to reproduce the experimental reflectivity data.

Experimental Setup. A custom PTFE trough with an area of of 240 × 70 mm^2 and a liquid depth of approximately 3.5 mm was used in the study. UV lamps were suspended above the trough along its length to photolytically generate the radicals and provide an even illumination of the air−solution interface. Two types of UV lamps were used, black lamps centered at wavelength ∼360 nm (UVP) to generate $SO_4^{\bullet-}$ and $NO_3^{\bullet}$ radicals and germicidal lamps that provided a significant output at ∼254 nm (UVP) to generate $^{\bullet}OH$ radicals. In both cases, the bulbs were situated in a retroreflector within the lamp body at a fixed height above the air−solution interface. The trough and lamps were loosely surrounded by a Tedlar plastic film to keep the interface free from dust.

A monolayer of fully deuterated DSPC ($C_{44}H_5NO_8PD_{83}$), >99% atom purity, from Avanti Polar Lipids Inc. was spread on the surface of the radical precursor aqueous subphase as a 1 mg mL^{-1} solution in chloroform (Sigma-Aldrich, 0.5−1% ethanol as stabilizer) using a glass microliter syringe. In each experiment, 40 μL was typically added to the air−solution interface. Previously it had been determined that 40 μL provided a surface pressure of ∼20 mN m^{-1} on the trough used in these experiments. Surface pressure was not measured during the neutron studies because UV radiation degrades the tensiometer and would have blocked the neutron beam on the small trough used to achieve even illumination from the photolysis lamp. Neutron reflectivity as a function of momentum transfer, Q, was recorded before and during photolysis of the subphase to monitor the change in the DSPC monolayer.[58,59]

Radical Generation. Aqueous radicals were photolytically produced from the subphase using aqueous phase photochemistry.[26,65−68] Hydroxyl radicals were generated by photolysis of a 0.03 mol dm^{-3} aqueous solution of KNO_3 by the method of Mack and Bolton[65] using two UV bulbs centered at ∼254 nm (UVP) and placed at a height of ∼83 mm above the trough. A clean well-established method of producing hydroxyl radicals as demonstrated by Karagulian et al.[43]

$$NO_3^-{}_{(aq)} + h\nu(\lambda \sim 254\ \text{nm}) \rightarrow NO_2^-{}_{(aq)} + O_{(aq)} \tag{R4}$$

$$NO_3^-{}_{(aq)} + h\nu(\lambda \sim 254\ \text{nm}) \rightarrow NO_{2(aq)} + O^{\bullet-}{}_{(aq)} \tag{R5}$$

$$O^{\bullet-}{}_{(aq)} + H_2O_{(aq)} \rightarrow OH_{(aq)} + OH^-{}_{(aq)} \tag{R6}$$

Sulfate radical anions were generated by photolysis of a 0.03 mol dm^{-3} aqueous solution of $K_2S_2O_8$[66] using four black bulbs

https://doi.org/10.1021/acs.jpca.3c03846
J. Phys. Chem. A 2023, 127, 8922−8934

centered at ~360 nm (UVP) at a height of 128 mm above the trough.

$$S_2O_8^{2-}{}_{(aq)} + h\nu(\lambda \sim 360\ \text{nm}) \rightarrow SO_4^{\bullet-}{}_{(aq)} + SO_4^{\bullet-}{}_{(aq)} \quad \text{(R7)}$$

Nitrate radicals were generated by photolysis of an aqueous solution subphase containing 0.03 mol dm^{-3} $K_2S_2O_8$ and 0.1 mol dm^{-3} KNO_3 by the method of Herrmann,[26] using four black bulbs centered at ~360 nm (UVP) and placed at a height of 128 mm above the trough at ISIS and 115 mm above the trough at the ILL. The height of the lamps was used to control the flux of photons and associated rate of reaction. Photolysis of $S_2O_8^{2-}$ yielded two $SO_4^{\bullet-}$ radicals as detailed in eq R7 and subsequent titration of $SO_4^{\bullet-}$ with an excess of NO_3^- resulted in the production of the nitrate radical, $NO_3^\bullet$ as described by Herrmann.[26]

$$SO_4^{\bullet-}{}_{(aq)} + NO_3^-{}_{(aq)} \rightarrow NO_3^\bullet{}_{(aq)} + SO_4^{2-}{}_{(aq)} \quad \text{(R8)}$$

The UV lamps used to initiate photolysis were switched on and off remotely and produced a stable irradiance after 3 min.[69] The concentration of the aqueous radical precursor was chosen to maintain a constant steady-state radical concentration throughout the entire kinetic run. The focus is on the radicals generated, not the radical precursors used, with the only requirement being that the precursors do not interfere with the reaction.

Two sets of control experiments were performed, "dark controls" conducted without UV light on a monolayer of DSPC on the aqueous solution subphases of 0.03 mol dm^{-3} KNO_3, 0.03 mol dm^{-3} $K_2S_2O_8$ with 0.1 mol dm^{-3} KNO_3, and 0.03 mol dm^{-3} $K_2S_2O_8$ and "light or photolysis controls" conducted with UV light on a monolayer of DSPC on null reflecting water with no radical precursors present.

Kinetic Modeling. Two kinetic models were developed in the work presented here: a multistep degradation of material at the air−solution interface and a steady-state analysis of the radical concentration. The secondary chemistry following photolysis required determination of the steady-state concentrations of hydroxyl radicals and sulfate radical anions by kinetic modeling as described below. It was not possible to attempt the same analysis and modeling with the nitrate radical as the secondary chemistry is not accurately known. Note that the steady-state analysis of the radical concentration ($^\bullet$OH, $NO_3^\bullet$ or $SO_4^{\bullet-}$) is strictly a determination of the "bulk" concentration of radical. The very large excess of the photolabile radical precursor (NO_3^- and $S_2O_8^{2-}$) should prevent a reduction in the radical concentration near the air−solution interface owing to reaction.

Determination of Radical Steady-State Concentrations. The steady-state concentrations were measured in a series of off-line experiments. The loss of radical precursor was measured as a function of photolysis time to determine the photolysis rate constant, J, for eqs R4, R5, and R7 offline. The offline experimental setup was the same as that used for the neutron reflectometry experiments. Kinetic modeling was required because the photolysis rates of the NO_3^- and $S_2O_8^{2-}$ anions were unknown. During the neutron reflectometry experiments, the concentration of radical precursors (NO_3^- and $S_2O_8^{2-}$) was kept large to maintain an effectively constant concentration of radical precursor and thus a constant concentration of radical in steady-state concentration throughout the reaction. However, in order to calculate the photolysis rate constant for NO_3^- and $S_2O_8^{2-}$ the precursor solutions were photolyzed at smaller concentrations of 0.0003 mol dm^{-3} KNO_3 aqueous solution and 0.0003 mol dm^{-3} $K_2S_2O_8$ aqueous solution to observe and model the loss of radical precursor. Loss of KNO_3 or $K_2S_2O_8$ was followed by UV−visible spectrometry for up to 10 h for $K_2S_2O_8$ and up to 16.5 h for KNO_3. The following photolysis reaction schemes were kinetically modeled using a Backward Differentiation Formula (BDF) method to handle stiff systems,[70−72] and the value of the appropriate photolysis rate constants, J, was varied until the modeled temporal variation of the concentrations of NO_3^-, NO_2^- and $S_2O_8^{2-}$ fitted the experimentally determined temporal profile of the concentrations. Rate constants for the reactions in the photolysis schemes were obtained from the literature where possible, and the following rate constants were determined from kinetic modeling: J_4, J_5, J_7, J_{11}, and k_{12}.

Hydroxyl radicals are produced from the photolysis of nitrate from the following photochemistry:

$$NO_3^-{}_{(aq)} + h\nu(\lambda \sim 254\ \text{nm}) \rightarrow NO_2^-{}_{(aq)} + O_{(aq)} \quad \text{(R4)}$$

$J_4 = 3.5 \times 10^{-6}\ s^{-1}$

$$NO_3^-{}_{(aq)} + h\nu(\lambda \sim 254\ \text{nm}) \xrightarrow{H_2O} NO_{2(aq)} + O^{\bullet-}{}_{(aq)} \quad \text{(R5)}$$

$J_5 = 3.5 \times 10^{-6}\ s^{-1}$

$$OH_{(aq)} + NO_3^-{}_{(aq)} \rightarrow NO_3^\bullet{}_{(aq)} + OH^-{}_{(aq)} \quad \text{(R9)}$$

$k_9 = 1.3 \times 10^8\ M^{-1}\ s^{-1}$[73]

$$OH_{(aq)} + NO_2^-{}_{(aq)} \rightarrow NO_2^\bullet{}_{(aq)} + OH^-{}_{(aq)} \quad \text{(R10)}$$

$k_{10} = 6.0 \times 10^9\ M^{-1}\ s^{-1}$[74]

$$NO_2^-{}_{(aq)} + h\nu(\lambda \sim 254\ \text{nm}) \xrightarrow{H_2O} NO^\bullet{}_{(aq)} + OH_{(aq)} \quad \text{(R11)}$$

$J_{11} = 5.0 \times 10^{-5}\ s^{-1}$

$$OH_{(aq)} + \text{wall} \rightarrow \quad \text{(R12)}$$

$k_{12} = 1\ s^{-1}$

$$NO_2^-{}_{(aq)} + NO_3^\bullet{}_{(aq)} \rightarrow NO_3^-{}_{(aq)} + NO_2^\bullet{}_{(aq)} \quad \text{(R13)}$$

$k_{13} = 6.0 \times 10^9\ M^{-1}\ s^{-1}$[74]

$$H_2O_{2(aq)} + h\nu \rightarrow OH_{(aq)} + OH_{(aq)} \quad \text{(R14)}$$

$k_{14} = 0$

$$OH_{(aq)} + H_2O_{2(aq)} \rightarrow H_2O_{(aq)} + HO_{2(aq)} \quad \text{(R15)}$$

$k_{15} = 4.2 \times 10^7\ M^{-1}\ s^{-1}$[75]

$$HO_{2(aq)} + H_2O_{2(aq)} \rightarrow O_{2(aq)} + OH_{(aq)} + H_2O_{(aq)} \quad \text{(R16)}$$

$k_{16} = 0.5\ M^{-1}\ s^{-1}$[75]

$$OH_{(aq)} + OH_{(aq)} \rightarrow H_2O_{2(aq)} \quad \text{(R17)}$$

$k_{17} = 6 \times 10^9\ M^{-1}\ s^{-1}$[75]

$$HO_{2(aq)} + HO_{2(aq)} \rightarrow H_2O_{2(aq)} + O_{2(aq)} \quad \text{(R18)}$$

$k_{18} = 980000\ M^{-1}\ s^{-1}$[75]

$$OH_{(aq)} + HO_{2(aq)} \rightarrow H_2O_{(aq)} + O_{2(aq)} \quad \text{(R19)}$$

https://doi.org/10.1021/acs.jpca.3c03846
J. Phys. Chem. A 2023, 127, 8922−8934

$k_{19} = 1.0 \times 10^{10}$ M^{-1} s^{-1}[75]

$$OH_{(aq)} + NO_{(aq)} \rightarrow NO_{2(aq)}^{-} + H^{+}_{(aq)} \quad (R20)$$

$k_{20} = 1.5 \times 10^{10}$ M^{-1} s^{-1}[65]

$$NO_{(aq)} + NO_{2(aq)} \rightarrow N_2O_{3(aq)} \quad (R21)$$

$k_{21} = 1.1 \times 10^{9}$ M^{-1} s^{-1}[65]

$$N_2O_{3(aq)} + H_2O_{(aq)} \rightarrow 2H^{+}_{(aq)} + 2NO_{2(aq)}^{-} \quad (R22)$$

$k_{22} = 530$ s^{-1}[65]

$$NO_{2(aq)} + NO_{2(aq)} \rightarrow N_2O_{4(aq)} \quad (R23)$$

$k_{23} = 4.5 \times 10^{8}$ M^{-1} s^{-1}[65]

$$N_2O_{4(aq)} + H_2O_{(aq)} \rightarrow NO_{2(aq)} + NO_{3(aq)} + 2H^{+}_{(aq)} \quad (R24)$$

$k_{24} = 1000$ s^{-1}[65]

$$OH_{(aq)} + NO_{2(aq)} \rightarrow HOONO_{(aq)} \quad (R25)$$

$k_{25} = 1.3 \times 10^{9}$ M^{-1} s^{-1}[65]

$$HOONO_{(aq)} + H_2O_{(aq)} \rightarrow NO_{3(aq)} + H^{+}_{(aq)} \quad (R26)$$

$k_{26} = 1.4$ s^{-1}[65]

The concentrations of NO_3^- and NO_2^- anions were measured by UV−visible spectrometry over the wavelength range ∼200−500 nm in a long path length liquid cell (17.5 cm) for a series of photolysis times from 2 h up to 16.5 h. The steady-state concentration of $^{\bullet}OH$ radicals was then determined from kinetically modeling the above reactions (reactions R4, R5, and R9−R26) as a series of first-order differential equations and varying J_4, J_5, J_{11}, and k_{12} to obtain a good fit between experimental and modeled $[NO_3^-]$ and $[NO_2^-]$ with time. The hydroxyl radical steady-state concentration was calculated from the precursor concentration used in the neutron experiments, 0.03 mol dm^{-3}, using the kinetic model as $\sim 1 \times 10^{-14}$ mol dm^{-3}.

The photolysis of persulfate, $K_2S_2O_8$ in aqueous solution leading to the production of sulfate radical anions derives from the following photochemistry:[73]

$$S_2O_8^{2-}{}_{(aq)} + h\nu(\lambda \sim 360\ nm) \rightarrow SO_4^{\bullet-}{}_{(aq)} + SO_4^{\bullet-}{}_{(aq)} \quad (R7)$$

$J_7 = 1.32 \times 10^{-5}$ s^{-1}

$$SO_4^{\bullet-}{}_{(aq)} + SO_4^{\bullet-}{}_{(aq)} \rightarrow S_2O_8^{2-}{}_{(aq)} \quad (R27)$$

$k_{27} = 6.1 \times 10^{8}$ M^{-1} s^{-1}[66]

$$SO_4^{\bullet-}{}_{(aq)} + S_2O_8^{2-}{}_{(aq)} \rightarrow SO_4^{2-}{}_{(aq)} + S_2O_8^{\bullet-}{}_{(aq)} \quad (R28)$$

$k_{28} = 5.5\times 10^{5}$ M^{-1} s^{-1}[66]

$$SO_4^{\bullet-}{}_{(aq)} + H_2O_{(aq)} \rightarrow H^{+}_{(aq)} + SO_4^{2-}{}_{(aq)} + OH^{\bullet}{}_{(aq)} \quad (R29)$$

$k_{29}[H_2O] = 460$ s^{-1}[66]

Owing to the weak absorption of the SO_4^{2-} anion, the decrease in concentration of $S_2O_8^{2-}$ was followed instead of the SO_4^{2-} anion as a function of photolysis time by UV−visible spectrometry over the wavelength range ∼200−300 nm. The steady-state concentration of $SO_4^{\bullet-}$ radicals was then determined from kinetically modeling the above reactions (reactions R7 and R27−R29) as a series of first-order differential equations and varying J_7. Similarly to steady-state [OH], denoted as $[OH]_{ss}$, once the photolysis rate constant, J_7, had been determined, the initial persulfate concentration (0.03 mol dm^{-3}) was used to calculate the sulfate radical steady-state concentration in the neutron experiments as 4.7×10^{-11} mol dm^{-3}.

It was noted that light attenuation by the water or aqueous radical precursor solution could occur at 254 or 360 nm; however, light attenuation was found not to be an issue following an e-folding depth calculation as detailed in the Supporting Information (Table S2).

RESULTS AND DISCUSSION

Figure 1 shows a typical decay in the neutron reflectivity profile with time as a monolayer film of DSPC at the air−solution interface is exposed to the aqueous phase hydroxyl radical. Note that not all reflectivity profiles are shown for clarity.

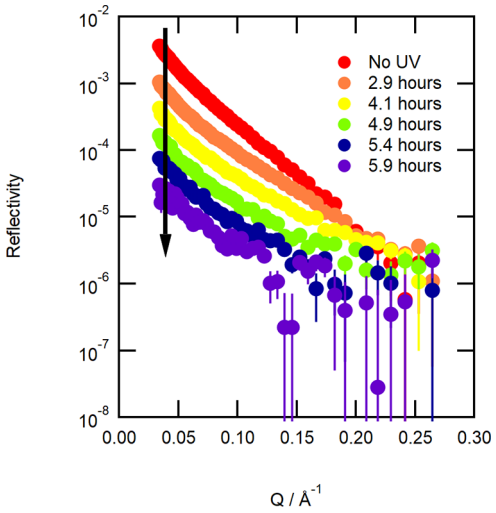

Figure 1. Typical neutron reflectivity profiles for a monolayer film of fully deuterated DSPC at the air−solution interface on exposure to the aqueous phase hydroxyl radical. The reflectivity of the film prior to exposure to the hydroxyl radical is the largest (red circles), and as the UV lights are switched on and the hydroxyl radical is generated, the reflectivity decreases in the direction of the black arrow to the purple circles (lowest reflectivity). Data were recorded on FIGARO.

Determination of Steady-State Radical Concentrations. The steady-state concentrations of reactant radicals listed in Table 1 were calculated by fitting the temporal decay of NO_3^-, NO_2^-, and $S_2O_8^{2-}$ as described in the determination of radical steady-state concentration in the experimental section and are shown in Figures S1 and S2 in the Supporting Information. Determination of the steady-state concentration was the largest source of uncertainty in the analysis. The concentration of OH radicals was sensitive to the photolysis rate constants (eqs R4, R5, and R11). Varying the value of these rate constants (eqs R4, R5, and R11) by a factor of ±40% led to a corresponding change in OH radical concentration of ±30%. Uncertainty analysis involved adjustment of the photolysis rate constants by fixed amounts and determination of the resultant steady-state concentration. From the analysis, both the hydroxyl and sulfate steady-state concentrations were determined to be within 40% of the values given in Table 1. Figure S3 shows the ±40% fit of the

https://doi.org/10.1021/acs.jpca.3c03846
J. Phys. Chem. A 2023, 127, 8922−8934

Table 1. Determined Values of Pseudo-First-Order and Bimolecular Rate Constants and Aqueous Steady-State Radical Concentrations for the Multistep Degradation Mechanism for the Aqueous Phase Hydroxyl and Sulfate Radical Systems[a]

Radical reaction	k' (10^{-4} s^{-1})	Steady-state radical concentration (mol dm^{-3})	k (mol^{-1} dm^3 s^{-1})[b]
$^{\bullet}OH$ R36	3.5	1×10^{-14}	3.5×10^{10}
$^{\bullet}OH$ R37	2.1	1×10^{-14}	2.1×10^{10}
$^{\bullet}OH$ R38	2.3	1×10^{-14}	2.3×10^{10}
$^{\bullet}OH$ R39	1.9	1×10^{-14}	1.9×10^{10}
$SO_4^{\bullet-}$ R36	2.22 ± 0.56	4.7×10^{-11}	$(3.77 \pm 2.15) \times 10^6$
$SO_4^{\bullet-}$ R37	1.85 ± 0.47	4.7×10^{-11}	$(3.93 \pm 0.99) \times 10^6$
$SO_4^{\bullet-}$ R38	1.85 ± 0.47	4.7×10^{-11}	$(3.93 \pm 0.99) \times 10^6$
$SO_4^{\bullet-}$ R39	1.85 ± 0.47	4.7×10^{-11}	$(3.93 \pm 0.99) \times 10^6$

[a]Average of the pseudo-first-order (reactions R36–R39) and bimolecular rate constants (determined using eq R44 and the modeled aqueous radical steady-state concentrations) for each degradation step in the multistep degradation mechanism for $^{\bullet}OH$ and $SO_4^{\bullet-}$, respectively. Two experiments were conducted using $^{\bullet}OH$, and hence no standard deviation is reported. [b]Note the diffusion limited bimolecular rate constant can be crudely estimated from $k = 8RT/(3\eta) \approx 6 \times 10^9$ M^{-1} s^{-1} assuming a temperature of 298 K and a viscosity of water, η, of 0.001 kg m^{-1} s^{-1}.[83]

photolysis rate constants for the hydroxyl radical as well as ±20, 60 and 80%. A ±40% variation in the photolysis rate constants corresponds to a ±30% variation in the OH steady-state concentration. The determination of the hydroxyl radical concentration was performed in a series of offline experiments. The apparatus, including lamps, scaffolding, trough, and chemicals, was exactly the same as the experimental apparatus used for determination of the kinetics of oxidation of the lipid. The only difference was that the concentration of radical precursor is lower in the offline experiments to allow the radical precursor concentration (nitrate anion or peroxydisulfate ion) to decrease and be measured in order to determine the photolysis rate coefficients of the precursor species. In some aspects the offline steady-state determination experiments are similar to a traditional actinometry experiment[76] but using the compound of photolysis as the actinometer.

Multistep Degradation Kinetics. It is useful to describe here the kinetic scheme used to model the decay of relative scattering length with the time of the organic layer at the air–solution interface. A multistep degradation mechanism[25,77] was fitted to the experimentally determined decrease in surface coverage of material with time at the air–solution interface. The characteristic temporal profile and lack of exponential decay led to consideration of a multistep degradation mechanism. The following mechanism is proposed:

$$DSPC_{(surf)} + X^{\bullet}_{(aq)} \rightarrow A_{(surf)} \rightarrow B_{(surf)} \rightarrow C_{(surf)} \rightarrow D_{(aq)} \quad (R30)$$

where $DSPC_{(surf)}$ is a monolayer of DSPC at the air–solution interface; $X^{\bullet}_{(aq)}$ is an aqueous radical oxidant (either $^{\bullet}OH$, $NO_3^{\bullet}$, or $SO_4^{\bullet-}$); $A_{(surf)}$, $B_{(surf)}$ and $C_{(surf)}$ are surface active deuterated products at the air–solution interface; and $D_{(aq)}$ is a deuterated product that is not surface-active, i.e., A, B, and C reside at the air–solution interface whereas product D partitions irreversibly to either the gas-phase or the aqueous subphase. Experimentally determined surface coverage was defined as the weighted sum of the surface coverage of all proposed deuterated product species at the air–solution interface including the original DSPC film and any other deuterated surface-active products that may have formed from reaction with the radical species, i.e., products A–C. Each proposed surface-active product (A–C) has a scattering length density that is consistent with oxidation removing parts of the original DSPC molecule (α, β, and γ in eq R31). It should be noted that the "true" mechanism will be more complicated as the number of products from the initial radical attack will be large. As such A, B, C, and D represent an ensemble of products, which have the typical scattering length density represented in eq R31. Thus, the total surface coverage at the air–solution interface determined by neutron reflection was defined as the weighted sum of Γ_{DSPC}, Γ_A, Γ_B, and Γ_C:

$$\Gamma_{tot} = \Gamma_{DSPC} + \alpha\Gamma_A + \beta\Gamma_B + \gamma\Gamma_C \quad (R31)$$

where α, β, and γ are the weightings relating to the scattering length density, ρ, of each surface-active decay product, i.e.,

$$\alpha = \frac{\rho_A}{\rho_{DSPC}} \quad (R32)$$

$$\beta = \frac{\rho_B}{\rho_{DSPC}} \quad (R33)$$

$$\gamma = \frac{\rho_C}{\rho_{DSPC}} \quad (R34)$$

Values of α, β, and γ were empirically taken as 0.95, 0.83, and 0.41 to represent stylized decay steps. The number of degradation steps and the values of α, β and γ were the result of trial and error during the fitting process and were selected to achieve a good fit between the model and experimental data.[78]

$$\Gamma_{tot} = \Gamma_{DSPC} + 0.95\Gamma_A + 0.83\Gamma_B + 0.41\Gamma_C \quad (R35)$$

As detailed below and in part 2 of the Supporting Information, a sensitivity study was performed on the number degradation steps and the values of α, β, and γ to ensure the use of optimum values that best described the temporal profile of the deuterated material at the interface. The experimentally determined surface coverage (eq E) as a function of reaction time was fitted to the following degradation scheme:

$$DSPC_{(surf)} + X^{\bullet}_{(aq)} \rightarrow A_{(surf)} \quad (R36)$$

$$A_{(surf)} + X^{\bullet}_{(aq)} \rightarrow B_{(surf)} \quad (R37)$$

$$B_{(surf)} + X^{\bullet}_{(aq)} \rightarrow C_{(surf)} \quad (R38)$$

$$C_{(surf)} + X^{\bullet}_{(aq)} \rightarrow D_{(aq)} \quad (R39)$$

where X = OH or $SO_4^{\bullet-}$, also a result of trial and error to obtain good agreement between the modeled and calculated temporal profiles of deuterated material at the air–solution interface.[78]

Reactions R36–R39 are modeled as a single reaction step with the OH radical. The single reaction represents significant well-known secondary chemistry[79] and may include autox-

https://doi.org/10.1021/acs.jpca.3c03846
J. Phys. Chem. A 2023, 127, 8922–8934

idation.[80−82] The determination of the value of rate constants for reactions R36−R39 may then represent an overestimation depending on the chain length[78] of the secondary chemical reactions. However, the secondary chemistry of the oxidation of single molecule thick films at the air−water interface is likely different from reactions within bulk organic particles of an aerosol. Unfortunately, the technique to study the kinetics described, while excellent for studies of monomolecular films at interfaces, does not produce the detailed chemical speciation to enable the secondary chemistry to be elucidated. Reactions of DSPC, A, B, and C with the OH radical (reactions R36−R39) may not be replaced by separate autoxidation events as demonstrated by switching off the photolysis lamp during reaction and noting a halt in the loss of material (neutron scattering length per unit area) from the air−solution interface. Reactions R36−R39 therefore suggest the removal of a molecule from a film of DSPC and its reaction products from the air−solution interface, consistent with approximately four radical attacks from photolytically generated radicals. The reactions R36−R39 have the following rate laws:[78]

$$\frac{d\Gamma_{DSPC}}{dt} = -k_{36}\Gamma_{DSPC}[X] \quad (R40)$$

$$\frac{d\Gamma_{A}}{dt} = k_{36}\Gamma_{DSPC}[X] - k_{37}\Gamma_{A}[X] \quad (R41)$$

$$\frac{d\Gamma_{B}}{dt} = k_{37}\Gamma_{A}[X] - k_{38}\Gamma_{B}[X] \quad (R42)$$

$$\frac{d\Gamma_{C}}{dt} = k_{38}\Gamma_{B}[X] - k_{39}\Gamma_{C}[X] \quad (R43)$$

The concentration of the radicals [X] in the vicinity of the air−solution interface are in steady-state during the reaction, i.e., $d[X]/dt = 0$, thus a series of pseudo-first-order rate constants, k', can be defined as:

$$k'_n = k_n[X] \quad (R44)$$

where n = 36, 37, 38, and 39 and eqs R40−R43 become:

$$\frac{d\Gamma_{DSPC}}{dt} = -k'_{36}\Gamma_{DSPC} \quad (R45)$$

$$\frac{d\Gamma_{A}}{dt} = k'_{36}\Gamma_{DSPC} - k'_{37}\Gamma_{A} \quad (R46)$$

$$\frac{d\Gamma_{B}}{dt} = k'_{37}\Gamma_{A} - k'_{38}\Gamma_{B} \quad (R47)$$

$$\frac{d\Gamma_{C}}{dt} = k'_{38}\Gamma_{B} - k'_{39}\Gamma_{C} \quad (R48)$$

Equations R32−R35 were kinetically modeled using a Runge−Kutta method,[70] and values of the pseudo-first-order rate constants were varied until the modeled temporal variation of the total surface coverage, Γ_{tot}, eq R35 fitted the experimentally determined temporal profile of surface coverage for each neutron experiment. The fitting of the kinetic eqs R36—R39 to the decay of $\frac{\rho\delta}{\rho_0\delta_0}$ versus time, by kinetic modeling a series of first-order differential rate laws is dependent on the number of degradation steps and the values of α, β and γ. A sensitivity study in part 2 of the Supporting Information describes how a chi-squared fitting parameter was used as a metric of the goodness of fit between the modeled and experimentally derived data for $\frac{\rho\delta}{\rho_0\delta_0}$ versus time as the number of degradation steps and values of α, β and γ were varied. While the sensitivity study does not explore the entirety of a large parameter space, it gives confidence that the values of α, β, and γ provide a good fit and that the minimum number of degradation steps are included. Note in the above analysis that the very slow diffusion of oxidized organic materials from the interface has not been considered, (diffusion on the time scale of tens of minutes to move 2.5 nm[62]). To estimate the possibility of such a process would require repeating the experiments, stopping the oxidation (by switching off the photolysis lamps) at periodic parts of the reaction, and observing/measuring any further loss of material.

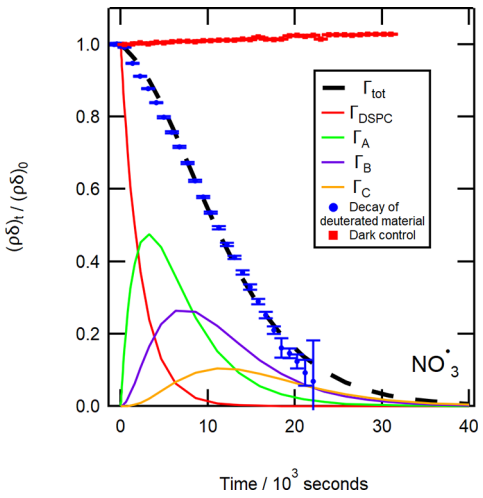

Figure 2. Experimental decay in relative surface coverage due to $NO_3^{\bullet}$ radicals is shown as blue circles. The modeled fit of the degradation mechanism to the experimental data is shown as the dashed black line. The remaining curves represent the decay of the initial DSPC film (red line) and the build-up and decay of the individual reaction products, A, B, and C. A dark control (no light, red squares), confirms that the reaction required the presence of UV light. It is thought that the gentle rise may be related to changes in the meniscus of the liquid surface as the reaction progressed. Data were recorded on FIGARO.

Figures 2, 3, and 4 show the experimental decays ($\frac{\rho\delta}{\rho_0\delta_0}$ versus time) of a monolayer film of DSPC on exposure to the aqueous phase radicals $NO_3^{\bullet}$, $SO_4^{\bullet-}$, and $^{\bullet}OH$, respectively. The experimental data are reproduced by calculation of eq R35 by varying the values of k'_{36}−k'_{39} using kinetic modeling. Table 1 highlights the modeled values of k' for each degradation step for each radical system ($^{\bullet}OH$ and $SO_4^{\bullet-}$).

Figures 2, 3, and 4 demonstrate a key result that the surface coverage of material at the air−solution interface can follow a multistep degradation mechanism.[78] Individual amounts of the modeled surface-active degradation products A, B, and C are also shown in Figures 2, 3, and 4 as well as control runs, which emphasize the difference between degradation and no reaction. Figure 2 includes a dark control, a monolayer film of DSPC on a radical precursor subphase with no light source, i.e., no photolysis. Figures 3 and 4 both show light controls, i.e., photolysis only, for a monolayer film of DSPC on NRW with UV light centered at ∼360 and 254 nm, respectively.

https://doi.org/10.1021/acs.jpca.3c03846
J. Phys. Chem. A 2023, 127, 8922−8934

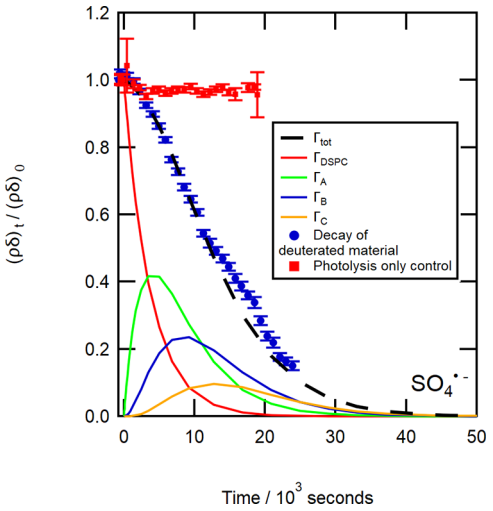

Figure 3. Experimental decay in relative surface coverage due to $SO_4^{\bullet -}$ radicals is shown as blue circles. The modeled fit of the degradation mechanism to the experimental data is shown as the dashed black line. The remaining curves represent the decay of the initial DSPC film (red line) and the build-up and decay of the individual reaction products. A photolysis control (~360 nm light, red squares) confirms minimal degradation of the film occurs owing to the presence of UV light. Data were recorded on SURF.

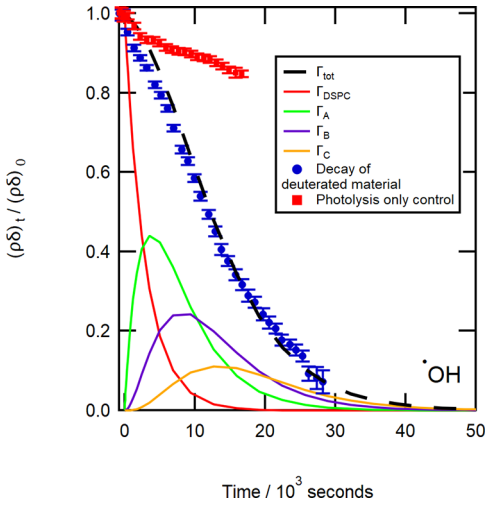

Figure 4. Experimental decay in relative surface coverage due to $^{\bullet}OH$ radicals is shown as blue circles. The modeled fit of the degradation mechanism to the experimental data is shown as a dashed black line. The remaining curves show the decrease in relative surface coverage of a monolayer film of DSPC (red) and the build-up and decrease in relative surface coverage of the reaction products. A photolysis control (~254 nm light, red squares), confirms some degradation of the film does occur owing to the presence of UV light. Data were recorded on SURF.

A simple exponential decay has been fitted to the photolysis control (red squares) in Figure 3, which is indicative of a very slow decay in relative surface coverage with time. A decay of ~4% in relative surface coverage in ~5.3 h is attributed to a small degradation owing to the presence of UV light only (centered at ~360 nm) demonstrating that UV radiation alone is not responsible for the loss of material from the interface.

Figure 4 shows the decrease on exposure to the aqueous hydroxyl radical. A ~71% decrease in the relative surface coverage was observed after 5 h of photolysis (~254 nm). As in Figure 3, there was a slight decrease in the amount of material for the photolysis control (red squares), so an exponential function was fitted to the decay. The exponential function indicated a ~15% decay in the initial relative surface coverage during ~5 h of exposure to UV light (~254 nm), which was a greater decay than that observed for the light control (~360 nm) in Figure 3. Comparing the decay from the light control to the decay observed for the radical reaction after 5 h of photolysis, the amount of deuterated material at the air–solution interface had decayed to ~64% of its initial value.

The pseudo-first-order and bimolecular rate constants reported in Table 1 are averaged for each degradation step for all of the experiments conducted using the aqueous sulfate radical. No uncertainties are reported for the hydroxyl system, as only two experiments were successful and neutron beam time is a very limited resource. All the pseudo-first-order rate constants for each radical system were also varied by factors of 5%, and the resultant fit through the experimental data points assessed by inspection. Variation of k' that provided a reasonable fit by eye was ±5% for the hydroxyl system, ±10% for the sulfate system, and ±20% for the nitrate system. For the nitrate system, a further sensitivity analysis was performed; each pseudo-first-order rate constant was varied individually by 10% and the remaining rate constants were subsequently adjusted to maintain a good fit through the data points. From variation of individual pseudo-first-order rate constants, it was deemed that no one rate constant was more or less significant in determining the reaction profile.

The diffusion of OH radicals to the interface was not considered to be a slow process relative to the rate of loss of OH radicals owing to reaction with the film. Characteristic time scales for diffusion and reaction can be estimated from simple formulas in Finlayson-Pitts and Pitts.[84] The characteristic time for transport of OH radicals to the interface is $\frac{d^2}{\pi^2 D}$, where d = 2.5 nm (the approximate size of the DSPC molecule at the air–water interface[62]) and an estimate of the diffusion coefficient $D = 2.8 \times 10^{-9}$ m^2 s^{-1}[85] gives ~0.2 ns. The characteristic reaction time is $\frac{1}{k}$ where $k = 3.5 \times 10^{-4}$ s^{-1} taken from Table 1 which gives a value with respect to reaction at the interface as ~3000 s. A detailed mass-transfer calculation or multilayer diffusion model as described elsewhere[86,87] is thus not considered. The photolytic source of OH radicals from an enormous excess of nitrate anions was chosen to prevent a diffusive concentration profile from building up to the interface over the course of the long reaction time.

Bimolecular Rate Constants. The bimolecular rate constants determined for each step in the degradation mechanism (eqs R36–R39) of a DSPC film initiated by aqueous phase $^{\bullet}OH$ radical attack are larger than the bimolecular rate constants determined for oxidation initiated by aqueous phase sulfate radical attack. Comparable values of bimolecular rate constants were determined in recent studies for aqueous phase $^{\bullet}OH$ radical reactions with *cis*-pinonic acid (~3–4 × 10^9 M^{-1} s^{-1}) and substituted phenols (on order of 10^9 M^{-1} s^{-1} to 10^{10} M^{-1} s^{-1} depending on the specific phenol and the pH).[88−90] The subsequent bimolecular rate constants for each step of the degradation mechanism are similar to each other, which is what is expected given that A, B, and C will have similar reactivity toward OH radical, i.e., the radical abstracts a deuterium from DPSC, A, B, and C.

Note that owing to the deuteration of the DSPC film for the neutron reflection technique, there will be a potential kinetic

https://doi.org/10.1021/acs.jpca.3c03846
J. Phys. Chem. A 2023, 127, 8922−8934

isotope effect on the values of the rate constants. Statistical mechanics has shown the kinetic isotope effect to be up to a factor of 7.2 for hydrogen abstraction,[78] but the kinetic isotope effect is generally a factor of 6.1 for breaking a C−H bond.[78] The rate constants have not been corrected for the kinetic isotope effect, and thus, the values in Table 1 represent a slight overestimation for atmospheric studies where the molecules would be predominately undeuterated. Note that a small proportion of our OH radicals will actually be OD radicals. The kinetic isotope effect of having some OD radicals is not considered important.

Comparison to Other Literature Studies. There have been several studies on the oxidation of thin films by gaseous phase oxidants, e.g. refs 25,35,53−55,91−94. Few studies have focused on oxidation of thin films from the aqueous phase;[44] however, an increasing number of recent studies focus on aqueous phase oxidation in the bulk[88,89,95−100,90,101] and in particular by the aqueous phase OH radical.[88−90,95,96,99−101] Other relevant studies include that of Sarang et al.,[97] who considered aqueous phase oxidation of so-called "Green Leaf Volatiles", unsaturated oxygenated hydrocarbons (volatile species emitted from plants that can partition into water), by $^{\bullet}OH$, $SO_4^{\bullet-}$, and $NO_3^{\bullet}$, and that of Tran et al.,[98] who studied oxidation by the aqueous phase $SO_4^{\bullet-}$ of a number of organic aerosol compounds including isoprene related compounds, lactic and pyruvic acid.

The second-order rate constants determined in the current study for oxidation by aqueous phase $^{\bullet}OH$ are on the order of 10^{10} M^{-1} s^{-1} and are comparable to other studies of aqueous phase $^{\bullet}OH$ bimolecular constants.[88−90] Relevant to this study is the study by Witkowski and Gierczak[88] who determined rate constants on the order 10^9 M^{-1} s^{-1} for reaction of aqueous phase $^{\bullet}OH$ and cis-pinonic acid. Similar values of bimolecular rate constants to those presented in Table 1 were also determined for the aqueous phase $^{\bullet}OH$ oxidation of substituted phenols.[89,90] Arciva et al.[90] determined second-order rate constants on the order of 10^9−10^{10} M^{-1} s^{-1} for the reaction of highly substituted phenols with the aqueous phase $^{\bullet}OH$, and He et al.[89] determined rate constants on the order of 10^9 M^{-1} s^{-1} for reaction of aqueous phase $^{\bullet}OH$ with methoxyphenolic compounds. Additionally, such reactions have been suggested as an important source of aqueous secondary organic aerosol, SOA.[90,102]

As discussed in the Introduction, Karagulian et al.[43] studied oxidation from the "bottom up" using OH radicals to oxidize a lipid, 1-oleoyl-2-palmitoyl-*sn*-glycero-3-phosphocholine (OPPC), coating on a solid mixture of NaCl and $NaNO_2$ particles. The chemistry observed in the work presented here, i.e., oxidation of a lipid from below in the aqueous phase, supports their hypothesis that such reactions could also occur on aqueous droplets coated in an organic film.

The aqueous phase oxidation temporal profiles of DSPC shown here (Figures 2−4) match those of DSPC and gas phase OH radicals,[25] suggesting that DSPC reacting with OH from the gaseous phase and the aqueous phase have similar chemical mechanisms. Further comparison of the kinetic profile observed in the current study with those of real film material abstracted from the atmosphere to the aqueous-phase OH and nitrate radical[44] also indicates a similar temporal profile. Thus, aqueous phase oxidation may preferentially proceed via a multistep degradation mechanism as described in the current work, but more studies on real atmospheric samples are required to confirm this. Additionally, the mechanism may be used to describe the aqueous phase radical induced oxidation of other saturated lipids, including those with different head groups.

Atmospheric Implications. The lifetime of a monomolecular film of DSPC at the air−solution interface with respect to aqueous phase $^{\bullet}OH$ radical attack was estimated to be ∼20 h using the following equation.

$$\tau = \frac{1}{k[\mathrm{OH}]} \tag{R49}$$

where [OH] is an atmospheric steady state concentration of aqueous $^{\bullet}OH$ radicals given as 3.80×10^{-16} mol dm^{-3}.[103] Typical atmospheric concentrations for $NO_3^{\bullet}$ and $SO_4^{\bullet-}$ are not readily available; therefore, the lifetime of DSPC with respect to $NO_3^{\bullet}$ and $SO_4^{\bullet-}$ was not calculated.

The lifetime of DSPC is interesting because it provides a measure of the importance of a lipid coating on atmospheric aerosol. A long-lived lipid (>4−10 days[3]) may not need to be considered in atmospheric oxidation models suggesting that it should be readily found in atmospheric filter samples. The short atmospheric lifetime (<4−10 days[3]) calculated above would suggest that the oxidation chemistry described here is important for atmospheric oxidation modeling. The amount of DSPC measured in atmospheric filters may be less than that released to the environment, as the lifetime is short enough for DSPC to have been partially removed in the atmosphere before being captured on a filter. The lifetime calculated in eq R49 is for DSPC. However, the work presented here has shown that products of reaction R1 remain at the air−solution interface and it is this product film, not just the DSPC, that affects light scattering and evaporation as well as other important processes of atmospheric aerosols. Thus, determination of the film lifetime may be more important than the DSPC lifetime, i.e., the time to remove DSPC and all its reaction products that favor the air−solution interface.

The differential equations used to describe the degradation mechanism were solved analytically (see part 3 of Supporting Information) and the relative amount of the film at the air−solution interface with time was estimated using the bimolecular rate constants listed in Table 1 and $^{\bullet}OH$ concentrations of 3.80×10^{-17} mol dm^{-3}, 3.80×10^{-16} mol dm^{-3},[103] and 3.80×10^{-15} mol dm^{-3} to provide an envelope of film lifetimes. These $^{\bullet}OH$ concentrations bracket the range of atmospheric $^{\bullet}OH$ (aq) concentrations determined in the literature,[104−107] and the estimated film lifetime is sensitive to these values. The estimated film lifetimes are shown in Figure 5, and the dotted vertical line corresponds to an estimate of the film half-life. Note that the film lifetime is different from the natural lifetime calculation in eq R49 (the characteristic time for the amount of DSPC to fall to $1/e$ of its initial value).

The solid black line in Figure 5 ($^{\bullet}OH$ concentration, 3.80×10^{-16} mol dm^{-3}) indicates that it takes ∼4−5 days for the amount of film material to decay to half of its initial amount, which is of the same order of magnitude as a typical aqueous aerosol lifetime and therefore suggests that oxidation initiated by the $^{\bullet}OH$ radical may be important to film lifetime in the atmosphere. The vertical dashed line emphasizes the film half-lives and indicates that the oxidation of the film depends on the $^{\bullet}OH$ radical concentration. An $^{\bullet}OH$ concentration of 3.80×10^{-15} mol dm^{-3} gives a half-life of ∼1/2 days whereas an $^{\bullet}OH$ concentration of 3.80×10^{-17} mol dm^{-3} gives a half-life greater than 50 days which is atmospherically unimportant. Thus the atmospheric importance of aqueous $^{\bullet}OH$ oxidation is

https://doi.org/10.1021/acs.jpca.3c03846
J. Phys. Chem. A 2023, 127, 8922−8934

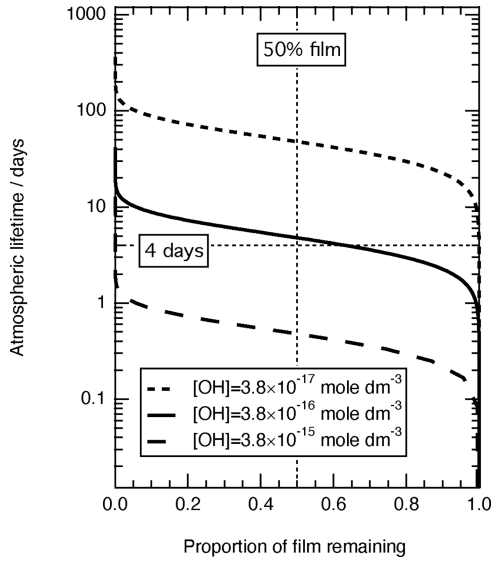

Figure 5. Atmospheric lifetime of the film versus proportion of the film remaining for three different •OH radical concentrations. The vertical dashed line highlights the atmospheric half-life. The importance of the •OH concentration is emphasized in the figure by considering that a typical aerosol lifetime is on the order of a few days.

very sensitive to •OH concentrations in particles in the atmosphere. Few studies of ambient •OH in droplets have been conducted.[103]

CONCLUSIONS

The amount of deuterated material at the air−solution interface was observed to decay when a monolayer film of the fully deuterated lipid DSPC was exposed to the aqueous phase radicals •OH, $SO_4^{\bullet-}$, and $NO_3^{\bullet}$. The decay was consistent with a multistep degradation mechanism with some products remaining at the air−solution interface that were subsequently oxidized by the aqueous radicals. Thus, lipid films on atmospheric aerosol will require several radical reaction steps to remove all organic material from the interface and atmospheric aqueous phase oxidation of lipid films at the air−solution interface can be described by multistep kinetics.

An atmospheric lifetime of ∼20 h was calculated for a DSPC molecule with respect to attack by an aqueous phase hydroxyl radical using a typical atmospheric concentration of aqueous hydroxyl radicals. The overall film lifetime was determined to have a half-life of ∼4−5 days, calculated using the literature concentration of 3.80×10^{-16} mol dm^{-3} for aqueous hydroxyl radicals.[103] Oxidation of thin films in the atmosphere by aqueous radicals may therefore be important, and reactions of lipid films appear consistent with a multistep degradation mechanism.

ASSOCIATED CONTENT

Supporting Information

The Supporting Information is available free of charge at https://pubs.acs.org/doi/10.1021/acs.jpca.3c03846.

Neutron reflectometry experiments conducted, e-folding depth, calculated steady state concentrations for thehydroxyl radical and sulfate anion, uncertainty in steady state hydroxyl radical concentration, sensitivity study of the number of steps and weighting constants used in the degradation kinetic modeling, and analytical solutions to the concentration−time profiles for the degradation mechanism used (PDF)

AUTHOR INFORMATION

Corresponding Authors

Stephanie H. Jones − *Centre of Climate, Ocean and Atmosphere, Department of Earth Sciences, Royal Holloway University of London, Egham, Surrey TW20 0EX, U.K.; STFC, Central Laser Facility, Research Complex at Harwell, Rutherford Appleton Laboratory, Didcot, Oxfordshire OX11 0FA, U.K.;* Present Address: Karlsruhe Institute of Technology (KIT), Institute of Meteorology and Climate Research, Atmospheric Aerosol Research Department, Hermann-von-Helmholtz-Platz 1, 76344 Eggenstein-Leopoldshafen, Germany; orcid.org/0000-0003-4493-0683; Email: stephanie.jones@kit.edu

Martin D. King − *Centre of Climate, Ocean and Atmosphere, Department of Earth Sciences, Royal Holloway University of London, Egham, Surrey TW20 0EX, U.K.;* orcid.org/0000-0002-0089-7693; Email: m.king@rhul.ac.uk

Authors

Adrian R. Rennie − *Department of Chemistry, Angström Laboratory, Uppsala University, 75121 Uppsala, Sweden;* orcid.org/0000-0001-8185-3272

Andrew D. Ward − *STFC, Central Laser Facility, Research Complex at Harwell, Rutherford Appleton Laboratory, Didcot, Oxfordshire OX11 0FA, U.K.;* orcid.org/0000-0001-6946-2391

Richard A. Campbell − *Institut Laue-Langevin, F-38042 Cedex 9 Grenoble, France;* Present Address: Division of Pharmacy & Optometry, Faculty of Medicine, Biology & Health, University of Manchester, Oxford Road, Manchester M13 9PT, United Kingdom.; orcid.org/0000-0002-6296-314X

Arwel V. Hughes − *ISIS Pulsed Neutron and Muon source, Rutherford Appleton Laboratory, Harwell Oxford, Oxfordshire OX11 0QX, U.K.*

Complete contact information is available at: https://pubs.acs.org/10.1021/acs.jpca.3c03846

Author Contributions

The manuscript was written through contributions of all authors. All authors have given approval to the final version of the manuscript.

Notes

The authors declare no competing financial interest.

ACKNOWLEDGMENTS

We thank STFC ISIS and the ILL for the award of beam time under the grants RB1320137, RB1310415, 9-10-1287, and 9-10-1288. S.H.J. is grateful to NERC for Ph.D. funding grant NE/H019103/1. M.D.K. wishes to acknowledge support from NERC NE/T00732X/1.

REFERENCES

(1) Saxena, P.; Hildemann, L. M. Water-Soluble Organics in Atmospheric Particles: A Critical Review of the Literature and Application of Thermodynamics to Identify Candidate Compounds. *J. Atmospheric Chem.* **1996**, *24* (1), 57−109.

(2) Pöschl, U. Atmospheric Aerosols: Composition, Transformation, Climate and Health Effects. *Angew. Chem., Int. Ed.* **2005**, *44* (46), 7520−7540.
(3) Pandis, S. N.; Wexler, A. S.; Seinfeld, J. H. Dynamics of Tropospheric Aerosols. *J. Phys. Chem.* **1995**, *99* (24), 9646−9659.
(4) Fuzzi, S.; Baltensperger, U.; Carslaw, K.; Decesari, S.; Denier van der Gon, H.; Facchini, M. C.; Fowler, D.; Koren, I.; Langford, B.; Lohmann, U.; et al. Particulate Matter, Air Quality and Climate: Lessons Learned and Future Needs. *Atmospheric Chem. Phys.* **2015**, *15* (14), 8217−8299.
(5) Goldstein, A. H.; Galbally, I. E. Known and Unexplored Organic Constituents in the Earth's Atmosphere. *Environ. Sci. Technol.* **2007**, *41* (5), 1514−1521.
(6) Gilman, J. B.; Tervahattu, H.; Vaida, V. Interfacial Properties of Mixed Films of Long-Chain Organics at the Air−Water Interface. *Atmos. Environ.* **2006**, *40* (34), 6606−6614.
(7) Masson-Delmotte, V., Zhai, P., Pirani, A., Connors, S. L., Péan, C., Berger, S., Caud, N., Chen, Y., Goldfarb, L., Gomis, M. I., et al., Eds. *Climate Change 2021: The Physical Science Basis. Contribution of Working Group I to the Sixth Assessment Report of the Intergovernmental Panel on Climate Change*. Cambridge University Press: Cambridge, United Kingdom, and New York, NY, USA, 2021, 2391 pp.
(8) Sun, J.; Ariya, P. A. Atmospheric Organic and Bio-Aerosols as Cloud Condensation Nuclei (CCN): A Review. *Atmos. Environ.* **2006**, *40* (5), 795−820.
(9) Donaldson, D. J.; Vaida, V. The Influence of Organic Films at the Air−Aqueous Boundary on Atmospheric Processes. *Chem. Rev.* **2006**, *106* (4), 1445−1461.
(10) Ellison, G. B.; Tuck, A. F.; Vaida, V. Atmospheric Processing of Organic Aerosols. *J. Geophys. Res. Atmospheres* **1999**, *104* (D9), 11633−11641.
(11) Davies, J. F.; Miles, R. E. H.; Haddrell, A. E.; Reid, J. P. Influence of Organic Films on the Evaporation and Condensation of Water in Aerosol. *Proc. Natl. Acad. Sci. U. S. A.* **2013**, *110* (22), 8807−8812.
(12) Eliason, T. L.; Gilman, J. B.; Vaida, V. Oxidation of Organic Films Relevant to Atmospheric Aerosols. *Atmos. Environ.* **2004**, *38* (9), 1367−1378.
(13) Gill, P. S.; Graedel, T. E.; Weschler, C. J. Organic Films on Atmospheric Aerosol Particles, Fog Droplets, Cloud Droplets, Raindrops, and Snowflakes. *Rev. Geophys.* **1983**, *21* (4), 903−920.
(14) Tervahattu, H.; Hartonen, K.; Kerminen, V.-M.; Kupiainen, K.; Aarnio, P.; Koskentalo, T.; Tuck, A. F.; Vaida, V. New Evidence of an Organic Layer on Marine Aerosols. *J. Geophys. Res. Atmospheres* **2002**, *107* (D7), 4053.
(15) Tervahattu, H.; Juhanoja, J.; Vaida, V.; Tuck, A. F.; Niemi, J. V.; Kupiainen, K.; Kulmala, M.; Vehkamäki, H. Fatty Acids on Continental Sulfate Aerosol Particles. *J. Geophys. Res. Atmospheres* **2005**, *110* (D6), D06207.
(16) Wyslouzil, B. E.; Wilemski, G.; Strey, R.; Heath, C. H.; Dieregsweiler, U. Experimental Evidence for Internal Structure in Aqueous−Organic Nanodroplets. *Phys. Chem. Chem. Phys.* **2006**, *8* (1), 54−57.
(17) Falkovich, A. H.; Schkolnik, G.; Ganor, E.; Rudich, Y. Adsorption of Organic Compounds Pertinent to Urban Environments onto Mineral Dust Particles. *J. Geophys. Res. Atmospheres* **2004**, *109* (D2), D02208.
(18) Russell, L. M.; Maria, S. F.; Myneni, S. C. B. Mapping Organic Coatings on Atmospheric Particles. *Geophys. Res. Lett.* **2002**, *29* (16), 26-1−26-4.
(19) Blanchard, D. C. Sea-to-Air Transport of Surface Active Material. *Science* **1964**, *146* (3642), 396−397.
(20) Donaldson, D. J.; George, C. Sea-Surface Chemistry and Its Impact on the Marine Boundary Layer. *Environ. Sci. Technol.* **2012**, *46* (19), 10385−10389.
(21) Simoneit, B. R. T. Organic Matter in Eolian Dusts over the Atlantic Ocean. *Mar. Chem.* **1977**, *5* (4), 443−464.
(22) Ruehl, C. R.; Wilson, K. R. Surface Organic Monolayers Control the Hygroscopic Growth of Submicrometer Particles at High Relative Humidity. *J. Phys. Chem. A* **2014**, *118* (22), 3952−3966.
(23) Forestieri, S. D.; Staudt, S. M.; Kuborn, T. M.; Faber, K.; Ruehl, C. R.; Bertram, T. H.; Cappa, C. D. Establishing the Impact of Model Surfactants on Cloud Condensation Nuclei Activity of Sea Spray Aerosol Mimics. *Atmospheric Chem. Phys.* **2018**, *18* (15), 10985−11005.
(24) Shepherd, R. H.; King, M. D.; Marks, A. A.; Brough, N.; Ward, A. D. Determination of the Refractive Index of Insoluble Organic Extracts from Atmospheric Aerosol over the Visible Wavelength Range Using Optical Tweezers. *Atmospheric Chem. Phys.* **2018**, *18* (8), 5235−5252.
(25) Shepherd, R. H.; King, M. D.; Rennie, A. R.; Ward, A. D.; Frey, M. M.; Brough, N.; Eveson, J.; Del Vento, S.; Milsom, A.; Pfrang, C.; et al. Measurement of Gas-Phase OH Radical Oxidation and Film Thickness of Organic Films at the Air−Water Interface Using Material Extracted from Urban, Remote and Wood Smoke Aerosol. *Environ. Sci. Atmospheres* **2022**, *2* (4), 574−590.
(26) Herrmann, H. Kinetics of Aqueous Phase Reactions Relevant for Atmospheric Chemistry. *Chem. Rev.* **2003**, *103* (12), 4691−4716.
(27) Herrmann, H.; Exner, M.; Jacobi, H.-W.; Raabe, G.; Reese, A.; Zellner, R. Laboratory Studies of Atmospheric Aqueous-Phase Free-Radical Chemistry: Kinetic and Spectroscopic Studies of Reactions of NO3 and SO4− Radicals with Aromatic Compounds. *Faraday Discuss.* **1995**, *100* (0), 129−153.
(28) Cappa, C. D.; Che, D. L.; Kessler, S. H.; Kroll, J. H.; Wilson, K. R. Variations in Organic Aerosol Optical and Hygroscopic Properties upon Heterogeneous OH Oxidation. *J. Geophys. Res. Atmospheres* **2011**, *116* (D15), D15204.
(29) Saxena, P.; Hildemann, L. M.; McMurry, P. H.; Seinfeld, J. H. Organics Alter Hygroscopic Behavior of Atmospheric Particles. *J. Geophys. Res. Atmospheres* **1995**, *100* (D9), 18755−18770.
(30) Asad, A.; Mmereki, B. T.; Donaldson, D. J. Enhanced Uptake of Water by Oxidatively Processed Oleic Acid. *Atmospheric Chem. Phys.* **2004**, *4* (8), 2083−2089.
(31) Eliason, T. L.; Aloisio, S.; Donaldson, D. J.; Cziczo, D. J.; Vaida, V. Processing of Unsaturated Organic Acid Films and Aerosols by Ozone. *Atmos. Environ.* **2003**, *37* (16), 2207−2219.
(32) Mircea, M.; Facchini, M. C.; Decesari, S.; Fuzzi, S.; Charlson, R. J. The Influence of the Organic Aerosol Component on CCN Supersaturation Spectra for Different Aerosol Types. *Tellus B* **2022**, *54* (1), 74−81.
(33) King, M. D.; Thompson, K. C.; Ward, A. D. Laser Tweezers Raman Study of Optically Trapped Aerosol Droplets of Seawater and Oleic Acid Reacting with Ozone: Implications for Cloud-Droplet Properties. *J. Am. Chem. Soc.* **2004**, *126* (51), 16710−16711.
(34) McFiggans, G.; Artaxo, P.; Baltensperger, U.; Coe, H.; Facchini, M. C.; Feingold, G.; Fuzzi, S.; Gysel, M.; Laaksonen, A.; Lohmann, U.; et al. The Effect of Physical and Chemical Aerosol Properties on Warm Cloud Droplet Activation. *Atmospheric Chem. Phys.* **2006**, *6* (9), 2593−2649.
(35) King, M. D.; Rennie, A. R.; Thompson, K. C.; Fisher, F. N.; Dong, C. C.; Thomas, R. K.; Pfrang, C.; Hughes, A. V. Oxidation of Oleic Acid at the Air−Water Interface and Its Potential Effects on Cloud Critical Supersaturations. *Phys. Chem. Chem. Phys.* **2009**, *11* (35), 7699−7707.
(36) Lim, C. Y.; Browne, E. C.; Sugrue, R. A.; Kroll, J. H. Rapid Heterogeneous Oxidation of Organic Coatings on Submicron Aerosols. *Geophys. Res. Lett.* **2017**, *44* (6), 2949−2957.
(37) Thompson, A. M. The Oxidizing Capacity of the Earth's Atmosphere: Probable Past and Future Changes. *Science* **1992**, *256* (5060), 1157−1165.
(38) Andreae, M. O.; Crutzen, P. J. Atmospheric Aerosols: Biogeochemical Sources and Role in Atmospheric Chemistry. *Science* **1997**, *276* (5315), 1052−1058.
(39) George, I. J.; Vlasenko, A.; Slowik, J. G.; Broekhuizen, K.; Abbatt, J. P. D. Heterogeneous Oxidation of Saturated Organic Aerosols by Hydroxyl Radicals: Uptake Kinetics, Condensed-Phase

https://doi.org/10.1021/acs.jpca.3c03846
J. Phys. Chem. A 2023, 127, 8922−8934

Products, and Particle Size Change. *Atmospheric Chem. Phys.* **2007**, *7* (16), 4187−4201.
(40) Wayne, R. P.; Barnes, I.; Biggs, P.; Burrows, J. P.; Canosa-Mas, C. E.; Hjorth, J.; Le Bras, G.; Moortgat, G. K.; Perner, D.; Poulet, G.; et al. The Nitrate Radical: Physics, Chemistry, and the Atmosphere. *Atmospheric Environ. Part Gen. Top.* **1991**, *25* (1), 1−203.
(41) Herrmann, H.; Hoffmann, D.; Schaefer, T.; Bräuer, P.; Tilgner, A. Tropospheric Aqueous-Phase Free-Radical Chemistry: Radical Sources, Spectra, Reaction Kinetics and Prediction Tools. *ChemPhysChem* **2010**, *11* (18), 3796−3822.
(42) Canonica, S.; Kohn, T.; Mac, M.; Real, F. J.; Wirz, J.; von Gunten, U. Photosensitizer Method to Determine Rate Constants for the Reaction of Carbonate Radical with Organic Compounds. *Environ. Sci. Technol.* **2005**, *39* (23), 9182−9188.
(43) Karagulian, F.; Dilbeck, C. W.; Finlayson-Pitts, B. J. Unusual Oxidation of Organics at Interfaces from the Bottom Up and Atmospheric Implications. *J. Am. Chem. Soc.* **2008**, *130* (34), 11272−11273.
(44) Jones, S. H.; King, M. D.; Ward, A. D.; Rennie, A. R.; Jones, A. C.; Arnold, T. Are Organic Films from Atmospheric Aerosol and Sea Water Inert to Oxidation by Ozone at the Air-Water Interface? *Atmos. Environ.* **2017**, *161*, 274−287.
(45) Lee, A. K. Y.; Herckes, P.; Leaitch, W. R.; Macdonald, A. M.; Abbatt, J. P. D. Aqueous OH Oxidation of Ambient Organic Aerosol and Cloud Water Organics: Formation of Highly Oxidized Products. *Geophys. Res. Lett.* **2011**, *38* (11), L11805.
(46) Anastasio, C.; McGregor, K. G. Chemistry of Fog Waters in California's Central Valley: 1. In Situ Photoformation of Hydroxyl Radical and Singlet Molecular Oxygen. *Atmos. Environ.* **2001**, *35* (6), 1079−1089.
(47) Nomi, S. N.; Kondo, H.; Sakugawa, H. Photoformation of OH Radical in Water-Extract of Atmospheric Aerosols and Aqueous Solution of Water-Soluble Gases Collected in Higashi-Hiroshima, Japan. *Geochem. J.* **2012**, *46* (1), 21−29.
(48) Faust, B. C.; Anastasio, C.; Allen, J. M.; Arakaki, T. Aqueous-Phase Photochemical Formation of Peroxides in Authentic Cloud and Fog Waters. *Science* **1993**, *260* (5104), 73−75.
(49) Herrmann, H.; Exner, M.; Zellner, R. Reactivity Trends in Reactions of the Nitrate Radical (NO3) with Inorganic and Organic Cloudwater Constituents. *Geochim. Cosmochim. Acta* **1994**, *58* (15), 3239−3244.
(50) Lu, J. R.; Thomas, R. K.; Penfold, J. Surfactant Layers at the Air/Water Interface: Structure and Composition. *Adv. Colloid Interface Sci.* **2000**, *84* (1), 143−304.
(51) Penfold, J.; Thomas, R. K. The Application of the Specular Reflection of Neutrons to the Study of Surfaces and Interfaces. *J. Phys.: Condens. Matter* **1990**, *2* (6), 1369−1412.
(52) Campbell, R. A. Recent Advances in Resolving Kinetic and Dynamic Processes at the Air/Water Interface Using Specular Neutron Reflectometry. *Curr. Opin. Colloid Interface Sci.* **2018**, *37*, 49−60.
(53) King, M. D.; Rennie, A. R.; Pfrang, C.; Hughes, A. V.; Thompson, K. C. Interaction of Nitrogen Dioxide (NO2) with a Monolayer of Oleic Acid at the Air−Water Interface − A Simple Proxy for Atmospheric Aerosol. *Atmos. Environ.* **2010**, *44* (14), 1822−1825.
(54) Pfrang, C.; Sebastiani, F.; Lucas, C. O. M.; King, M. D.; Hoare, I. D.; Chang, D.; Campbell, R. A. Ozonolysis of Methyl Oleate Monolayers at the Air−Water Interface: Oxidation Kinetics, Reaction Products and Atmospheric Implications. *Phys. Chem. Chem. Phys.* **2014**, *16* (26), 13220−13228.
(55) King, M. D.; Jones, S. H.; Lucas, C. O. M.; Thompson, K. C.; Rennie, A. R.; Ward, A. D.; Marks, A. A.; Fisher, F. N.; Pfrang, C.; Hughes, A. V.; et al. The Reaction of Oleic Acid Monolayers with Gas-Phase Ozone at the Air Water Interface: The Effect of Sub-Phase Viscosity, and Inert Secondary Components. *Phys. Chem. Chem. Phys.* **2020**, *22* (48), 28032−28044.
(56) Garrett, W. D. The Organic Chemical Composition of the Ocean Surface. *Deep Sea Res. Oceanogr. Abstr.* **1967**, *14* (2), 221−227.
(57) Larsson, K.; Odham, G.; Södergren, A. On Lipid Surface Films on the Sea. I. A Simple Method for Sampling and Studies of Composition. *Mar. Chem.* **1974**, *2* (1), 49−57.
(58) Penfold, J.; Richardson, R. M.; Zarbakhsh, A.; Webster, J. R. P.; Bucknall, D. G.; Rennie, A. R.; Jones, R. a. L.; Cosgrove, T.; Thomas, R. K.; Higgins, J. S.; et al. Recent Advances in the Study of Chemical Surfaces and Interfaces by Specular Neutron Reflection. *J. Chem. Soc. Faraday Trans.* **1997**, *93* (22), 3899−3917.
(59) Campbell, R. A.; Wacklin, H. P.; Sutton, I.; Cubitt, R.; Fragneto, G. FIGARO: The New Horizontal Neutron Reflectometer at the ILL. *Eur. Phys. J. Plus* **2011**, *126* (11), 107.
(60) Sears, V. F. Neutron Scattering Lengths and Cross Sections. *Neutron News* **1992**, *3* (3), 26−37.
(61) Pynn, R. Neutron Scattering—A Non-Destructive Microscope for Seeing Inside Matter. In *Neutron Applications in Earth, Energy and Environmental Sciences*; Liang, L., Rinaldi, R., Schober, H., Eds.; Neutron Scattering Applications and Techniques; Springer US: Boston, MA, 2009; pp 15−36.
(62) Hollinshead, C. M.; Harvey, R. D.; Barlow, D. J.; Webster, J. R. P.; Hughes, A. V.; Weston, A.; Lawrence, M. J. Effects of Surface Pressure on the Structure of Distearoylphosphatidylcholine Monolayers Formed at the Air/Water Interface. *Langmuir* **2009**, *25* (7), 4070−4077.
(63) Abelès, F. La théorie générale des couches minces. *J. Phys. Radium* **1950**, *11* (7), 307−309.
(64) Nelson, A. Co-Refinement of Multiple-Contrast Neutron/X-Ray Reflectivity Data Using MOTOFIT. *J. Appl. Crystallogr.* **2006**, *39* (2), 273−276.
(65) Mack, J.; Bolton, J. R. Photochemistry of Nitrite and Nitrate in Aqueous Solution: A Review. *J. Photochem. Photobiol. Chem.* **1999**, *128* (1), 1−13.
(66) Yu, X.-Y.; Bao, Z.-C.; Barker, J. R. Free Radical Reactions Involving Cl•, Cl2-•, and SO4-• in the 248 Nm Photolysis of Aqueous Solutions Containing S2O82- and Cl-. *J. Phys. Chem. A* **2004**, *108* (2), 295−308.
(67) Chu, L.; Anastasio, C. Quantum Yields of Hydroxyl Radical and Nitrogen Dioxide from the Photolysis of Nitrate on Ice. *J. Phys. Chem. A* **2003**, *107* (45), 9594−9602.
(68) Chu, L.; Anastasio, C. Temperature and Wavelength Dependence of Nitrite Photolysis in Frozen and Aqueous Solutions. *Environ. Sci. Technol.* **2007**, *41* (10), 3626−3632.
(69) Lucas, C. Oxidation of Organic Films on Cloud Droplets, Doctoral Thesis, Royal Holloway, University of London, 2012, 420 pp.
(70) Press, W. H.; Flannery, B. P.; Teukolsky, S. A.; Vetterling, W. T. *Numerical Recipes in C: The Art of Scientific Computing*, 2nd ed.; Cambridge University Press: Cambridge, MA, 1992, 994 pp.
(71) Cohen, S.; Hindmarsh, A. C. *CVODE User Guide*, Technical Report UCRL-MA-118618, LLNL, 1994, 91 pp.
(72) Brown, P. N.; Byrne, G. D.; Hindmarsh, A. C. VODE: A Variable-Coefficient ODE Solver. *SIAM J. Sci. Stat. Comput.* **1989**, *10* (5), 1038−1051.
(73) Katsumura, Y.; Jiang, P. Y.; Nagaishi, R.; Oishi, T.; Ishigure, K.; Yoshida, Y. Pulse Radiolysis Study of Aqueous Nitric Acid Solutions: Formation Mechanism, Yield, and Reactivity of NO3 Radical. *J. Phys. Chem.* **1991**, *95* (11), 4435−4439.
(74) Loegager, T.; Sehested, K. Formation and Decay of Peroxynitric Acid: A Pulse Radiolysis Study. *J. Phys. Chem.* **1993**, *97* (39), 10047−10052.
(75) Yu, X.-Y.; Barker, J. R. Hydrogen Peroxide Photolysis in Acidic Aqueous Solutions Containing Chloride Ions. I. Chemical Mechanism. *J. Phys. Chem. A* **2003**, *107* (9), 1313−1324.
(76) Calvert, J. G.; Pitts, J. N. *Photochemistry*; Wiley: New York, 1967, 899 pp.
(77) Enami, S.; Hoffmann, M. R.; Colussi, A. J. Stepwise Oxidation of Aqueous Dicarboxylic Acids by Gas-Phase OH Radicals. *J. Phys. Chem. Lett.* **2015**, *6* (3), 527−534.
(78) Laidler, K. J. *Chemical Kinetics*; Harper & Row, 1987, 531pp.

https://doi.org/10.1021/acs.jpca.3c03846
J. Phys. Chem. A 2023, 127, 8922−8934

(79) Griffin, R. J.; Dabdub, D.; Seinfeld, J. H. Secondary Organic Aerosol 1. Atmospheric Chemical Mechanism for Production of Molecular Constituents. *J. Geophys. Res. Atmospheres* **2002**, *107* (D17), AAC 3-1.
(80) Crounse, J. D.; Nielsen, L. B.; Jørgensen, S.; Kjaergaard, H. G.; Wennberg, P. O. Autoxidation of Organic Compounds in the Atmosphere. *J. Phys. Chem. Lett.* **2013**, *4* (20), 3513−3520.
(81) Zhang, W.; Zhao, Z.; Shen, C.; Zhang, H. Unexpectedly Efficient Aging of Organic Aerosols Mediated by Autoxidation. *Environ. Sci. Technol.* **2023**, *57* (17), 6965−6974.
(82) Bianchi, F.; Kurtén, T.; Riva, M.; Mohr, C.; Rissanen, M. P.; Roldin, P.; Berndt, T.; Crounse, J. D.; Wennberg, P. O.; Mentel, T. F.; et al. Highly Oxygenated Organic Molecules (HOM) from Gas-Phase Autoxidation Involving Peroxy Radicals: A Key Contributor to Atmospheric Aerosol. *Chem. Rev.* **2019**, *119* (6), 3472−3509.
(83) Atkins, P. W.; De Paula, J. *Atkins' Physical Chemistry*, 7th ed.; Oxford University Press: Oxford, 2002. 1149 pp.
(84) Finlayson-Pitts, B. J.; Pitts, J. N. Kinetics and Atmospheric Chemistry. In *Chemistry of the Upper and Lower Atmosphere*; Finlayson-Pitts, B. J., Pitts, J. N., Eds.; Academic Press: San Diego, 2000; Chapter 5, pp 130−178.
(85) Codorniu-Hernández, E.; Kusalik, P. G. Mobility Mechanism of Hydroxyl Radicals in Aqueous Solution via Hydrogen Transfer. *J. Am. Chem. Soc.* **2012**, *134* (1), 532−538.
(86) Zhang, H.; Worton, D. R.; Shen, S.; Nah, T.; Isaacman-VanWertz, G.; Wilson, K. R.; Goldstein, A. H. Fundamental Time Scales Governing Organic Aerosol Multiphase Partitioning and Oxidative Aging. *Environ. Sci. Technol.* **2015**, *49* (16), 9768−9777.
(87) Milsom, A.; Lees, A.; Squires, A. M.; Pfrang, C. MultilayerPy (v1.0): A Python-Based Framework for Building, Running and Optimising Kinetic Multi-Layer Models of Aerosols and Films. *Geosci. Model Dev.* **2022**, *15* (18), 7139−7151.
(88) Witkowski, B.; Gierczak, T. *cis*-Pinonic Acid Oxidation by Hydroxyl Radicals in the Aqueous Phase under Acidic and Basic Conditions: Kinetics and Mechanism. *Environ. Sci. Technol.* **2017**, *51* (17), 9765−9773.
(89) He, L.; Schaefer, T.; Otto, T.; Kroflič, A.; Herrmann, H. Kinetic and Theoretical Study of the Atmospheric Aqueous-Phase Reactions of OH Radicals with Methoxyphenolic Compounds. *J. Phys. Chem. A* **2019**, *123* (36), 7828−7838.
(90) Arciva, S.; Niedek, C.; Mavis, C.; Yoon, M.; Sanchez, M. E.; Zhang, Q.; Anastasio, C. Aqueous $^{\bullet}$OH Oxidation of Highly Substituted Phenols as a Source of Secondary Organic Aerosol. *Environ. Sci. Technol.* **2022**, *56* (14), 9959−9967.
(91) Voss, L. F.; Bazerbashi, M. F.; Beekman, C. P.; Hadad, C. M.; Allen, H. C. Oxidation of Oleic Acid at Air/Liquid Interfaces. *J. Geophys. Res. Atmospheres* **2007**, *112* (D6), D06209.
(92) González-Labrada, E.; Schmidt, R.; DeWolf, C. E. Real-Time Monitoring of the Ozonolysis of Unsaturated Organic Monolayers. *Chem. Commun.* **2006**, *23*, 2471−2473.
(93) González-Labrada, E.; Schmidt, R.; DeWolf, C. E. Kinetic Analysis of the Ozone Processing of an Unsaturated Organic Monolayer as a Model of an Aerosol Surface. *Phys. Chem. Chem. Phys.* **2007**, *9* (43), 5814−5821.
(94) Thompson, K. C.; Jones, S. H.; Rennie, A. R.; King, M. D.; Ward, A. D.; Hughes, B. R.; Lucas, C. O. M.; Campbell, R. A.; Hughes, A. V. Degradation and Rearrangement of a Lung Surfactant Lipid at the Air−Water Interface during Exposure to the Pollutant Gas Ozone. *Langmuir* **2013**, *29* (14), 4594−4602.
(95) Schaefer, T.; Wen, L.; Estelmann, A.; Maak, J.; Herrmann, H. PH- and Temperature-Dependent Kinetics of the Oxidation Reactions of OH with Succinic and Pimelic Acid in Aqueous Solution. *Atmosphere* **2020**, *11* (4), 320.
(96) Wen, L.; Schaefer, T.; He, L.; Zhang, Y.; Sun, X.; Ventura, O. N.; Herrmann, H. T- and pH-Dependent Kinetics of the Reactions of $^{\bullet}$OH $_{(aq)}$ with Glutaric and Adipic Acid for Atmospheric Aqueous-Phase Chemistry. *ACS Earth Space Chem.* **2021**, *5* (8), 1854−1864.
(97) Sarang, K.; Otto, T.; Rudzinski, K.; Schaefer, T.; Grgić, I.; Nestorowicz, K.; Herrmann, H.; Szmigielski, R. Reaction Kinetics of Green Leaf Volatiles with Sulfate, Hydroxyl, and Nitrate Radicals in Tropospheric Aqueous Phase. *Environ. Sci. Technol.* **2021**, *55* (20), 13666−13676.
(98) Tran, L. N.; Abellar, K. A.; Cope, J. D.; Nguyen, T. B. Second-Order Kinetic Rate Coefficients for the Aqueous-Phase Sulfate Radical (SO4•−) Oxidation of Some Atmospherically Relevant Organic Compounds. *J. Phys. Chem. A* **2022**, *126* (37), 6517−6525.
(99) Yang, D.; Schaefer, T.; Wen, L.; Herrmann, H. Temperature- and PH- Dependent OH Radical Reaction Kinetics of Tartaric and Mucic Acids in the Aqueous Phase. *J. Phys. Chem. A* **2022**, *126* (36), 6244−6252.
(100) Wen, L.; Schaefer, T.; Zhang, Y.; He, L.; Ventura, O. N.; Herrmann, H. T- and pH-Dependent OH Radical Reaction Kinetics with Glycine, Alanine, Serine, and Threonine in the Aqueous Phase. *Phys. Chem. Chem. Phys.* **2022**, *24* (18), 11054−11065.
(101) Schaefer, T.; Herrmann, H. Competition Kinetics of OH Radical Reactions with Oxygenated Organic Compounds in Aqueous Solution: Rate Constants and Internal Optical Absorption Effects. *Phys. Chem. Chem. Phys.* **2018**, *20* (16), 10939−10948.
(102) Ervens, B.; Sorooshian, A.; Lim, Y. B.; Turpin, B. J. Key Parameters Controlling OH-Initiated Formation of Secondary Organic Aerosol in the Aqueous Phase (AqSOA). *J. Geophys. Res. Atmospheres* **2014**, *119* (7), 3997−4016.
(103) Anastasio, C.; Newberg, J. T. Sources and Sinks of Hydroxyl Radical in Sea-Salt Particles. *J. Geophys. Res. Atmospheres* **2007**, *112* (D10), D10306.
(104) Kaur, R.; Anastasio, C. Light Absorption and the Photoformation of Hydroxyl Radical and Singlet Oxygen in Fog Waters. *Atmos. Environ.* **2017**, *164*, 387−397.
(105) Kaur, R.; Labins, J. R.; Helbock, S. S.; Jiang, W.; Bein, K. J.; Zhang, Q.; Anastasio, C. Photooxidants from Brown Carbon and Other Chromophores in Illuminated Particle Extracts. *Atmospheric Chem. Phys.* **2019**, *19* (9), 6579−6594.
(106) Lallement, A.; Vinatier, V.; Brigante, M.; Deguillaume, L.; Delort, A. M.; Mailhot, G. First Evaluation of the Effect of Microorganisms on Steady State Hydroxyl Radical Concentrations in Atmospheric Waters. *Chemosphere* **2018**, *212*, 715−722.
(107) Anastasio, C.; McGregor, K. G. Chemistry of Fog Waters in California's Central Valley: 1. In Situ Photoformation of Hydroxyl Radical and Singlet Molecular Oxygen. *Atmos. Environ.* **2001**, *35* (6), 1079−1089.

https://doi.org/10.1021/acs.jpca.3c03846
J. Phys. Chem. A 2023, 127, 8922−8934